ELSEVIER

Journal of Power Sources 91 (2000) 107–117

JOURNAL OF POWER SOURCES

www.elsevier.com/locate/jpowsour

Palladium-microencapsulated graphite as the negative electrode in Li-ion cells

Ping Yu, Bala S. Haran, James A. Ritter, Ralph E. White, Branko N. Popov *

Department of Chemical Engineering, Center for Electrochemical Engineering, University of South Carolina, Columbia, SC 29208, USA

Received 19 October 1999; accepted 16 February 2000

Abstract

A Pd-encapsulated graphite electrode was used as the negative electrode in Li-ion cells. Through dispersion of ultrafine nanoparticles of palladium on the surface of graphite, the interfacial properties of the carbon surface were modified. The presence of the palladium dramatically reduces the initial irreversible capacity of the graphite in propylene carbonate (PC)-based electrolyte. Palladium suppresses the solvated lithium ion intercalation and improves the charge–discharge performance and initial coulombic efficiency of graphite. For example, 10-wt.% of Pd-nanoparticles dispersed on the surface of graphite increases the initial charge–discharge coulombic efficiency from 59% to 80.3%. Electrochemical impedance spectroscopy (EIS) indicates that palladium dispersed on graphite increases the ohmic conductivity and also improves the Li insertion rate into graphite. However, an excess amount of palladium on graphite leads to a decrease in the charge–discharge efficiency due to the consumption of lithium by the formation of Li_2PdO_2.

Keywords: Nanoparticles; Dispersed palladium; Irreversible capacity; Graphite; Lithium intercalation; Li-ion battery

1. Introduction

Various carbon-based materials have been widely investigated as the negative electrode in Li-ion batteries [1–5]. Of these materials, graphite is favored as the negative electrode because it is low-cost and exhibits a high specific capacity, the most desirable discharge potential profile and superior cycling life. However, a major problem associated with the use of graphite concerns the irreversible reactions that take place during the first charge (lithium intercalation). These reactions consume a significant amount of active material (Li) which leads to a loss in capacity that cannot be recovered during subsequent cycling. In commercial Li-ion cells, the loss of lithium due to the irreversible reactions is normally compensated for with the use of excess cathode material [6,7]. But this leads to a decrease in the specific energy density and thus an increase in the cell cost. Moreover, these irreversible reactions can cause gas evolution, which may result in safety problems such as cell can buckling, cell venting, electrolyte spillage, and even fire [6–8].

These irreversible reactions are also much worse in propylene carbonate (PC)-based electrolyte than in ethylene carbonate (EC)-based electrolyte [9–11] and PC alone can cause severe degradation of the graphite structure [4,9–11] by a process called “exfoliation” [2]. PC decomposes without forming a stable passive layer on the edge surface of graphite [4,9–11]; and hence, it continues to solvate with lithium ions, which then cointercalate and undergo a reduction reaction inside the graphene layers. These sequential events give rise to the large irreversible capacity associated with the use of PC-based electrolytes [8,11].

One common approach taken to improve the capacity of carbon in PC-based electrolytes is to modify existing carbons with dopants such as P, B and N. However, both the parasitic irreversible reaction and the Li intercalation reaction take place at the interface between the carbon and the electrolyte. Hence, no significant improvement in the properties of the graphite can be achieved unless the interfacial properties are improved. Recently, some efforts have focussed on modifying the surface of graphite to reduce electrolyte decomposition, especially that associ-

* Corresponding author. Tel.: +1-803-777-7314; fax: +1-803-777-8265.

E-mail address: popov@engr.sc.edu (B.N. Popov).

0378-7753/00/$ - see front matter
PII: S0378-7753(00)00466-3

ated with solvent cointercalation and decomposition [12–18]. For example, mild oxidation at high temperature removed unfavorable contaminants and formed carbonate functional groups on the graphite surface, which decreased the irreversible capacity. Another approach involved modifying the carbon surface with a thin metal film. For example, Takamura et al. [13,14] showed that a vacuum deposited palladium coating on carbon fiber markedly improved the lithium intercalation and deintercalation rates. Similarly, a thin film of gold vacuum deposited on carbon increased the doping/undoping current peaks [15]; and electroless deposition of silver on natural graphite powder enhanced the lithium electrochemical reaction [16,17]. Ultrafine silver particles dispersed on the surface of graphite also alleviated the capacity fade associated with carbon anodes [18].

Clearly, electroless deposition affords a unique way of modifying the surface of the substrate. Since, the above researchers reported promising results with vacuum deposition of Pd on carbon fibers, it was decided here to deposit Pd on the surface of graphite. Therefore, the objective of this work is to introduce a palladium-coated graphite electrode and to show that this coating also reduces the first cycle irreversible capacity in PC-based electrolytes. None of the aforementioned studies on metal-coated carbon electrodes considered the effect of the coating on the first cycle irreversible capacity.

Our previous study showed that nano-sized Ni-composite deposited on graphite significantly reduced the irreversible capacity by suppressing the solvated lithium intercalation and reduction [24]. This paper intends to investigate the behavior of palladium dispersed graphite. The palladium dispersed graphite electrode was fabricated by electroless plating of nanoparticles of palladium on graphite. The performance of this new composite material as the negative electrode in a Li-ion cell was compared to that of bare graphite based on galvanostatic charge–discharge, cyclic voltammetry (CV), and electrochemical impedance spectroscopy (EIS). Scanning electron microscopy (SEM) and powered X-ray diffraction (XRD) were also used to assist in revealing the effect of the metal coating on improving the performance of the graphite.

2. Experimental

In this study, SFG75 graphite (Timcal America) with a particle diameter of 75 μm was used. Prior to palladium deposition, the graphite was initially sensitized by immersing in an acidified 2 g/l $SnCl_2$ bath and subsequently activating in an acidified 2 g/l $PdCl_2$ bath. Palladium deposition (5 wt.%) on SFG75 was carried out in a plating solution containing 0.0877 g $PdCl_2$, 8.25 ml NH_4OH, 1.34 g NH_4Cl, 0.52 g $NaH_2PO_2 \cdot H_2O$, and 1 g SFG75 graphite with moderate stirring at 80–85°C. The pH of the plating solution was adjusted to 8.5–9.5 by using a dilute NH_4OH solution during the plating process. Using this process, different amounts of Pd nanoparticles (8, 10 and 25 wt.%) were deposited on SFG75. After deposition, the graphite was washed with deionized water and dried at 90°C in a vacuum oven for 12 h.

The electrochemical studies were carried out in Swagelok three-electrode T-cells assembled in an argon-blanketed glove box. A typical T-cell was prepared by mixing bare SFG75 or Pd-coated SFG75 graphite powder with 6 wt.% poly(vinylidene fluoride) (PVDF, Aldrich) in 1-methyl-2-pyrrolidinone solvent. The resulting slurry was spread onto a stainless steel current collector and dried under vacuum at 150°C for 12 h. This procedure produced an electrode containing approximately 10 mg of active material. The counter and reference electrodes were made of lithium foil (99.9%, Aldrich). A sheet of Whatman glass fiber membrane (Baxter) 0.3 mm thick was used as the

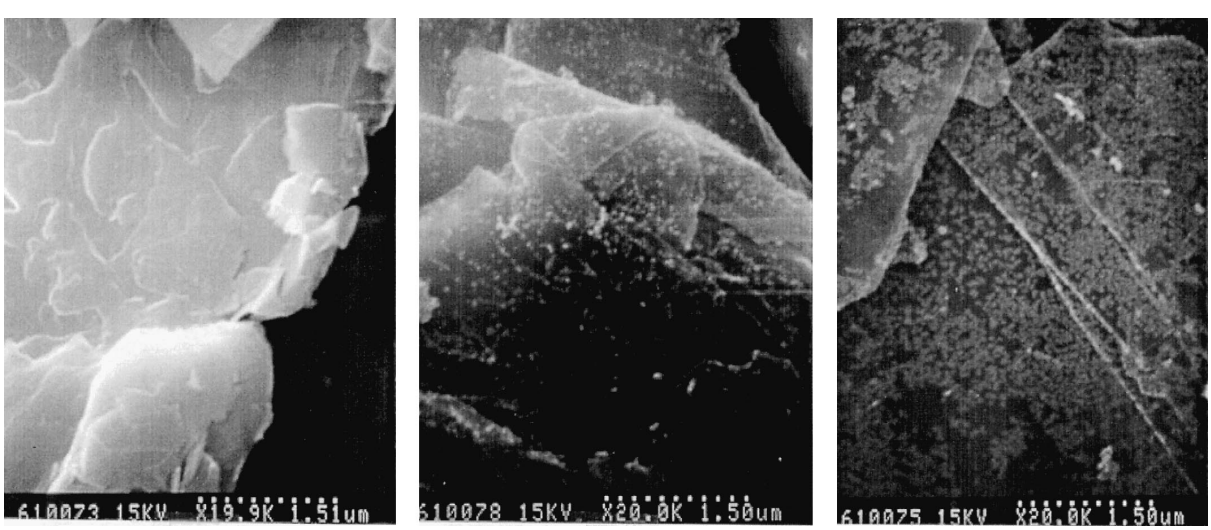

Fig. 1. SEM images for (a) bare, (b) 5 wt.% and (c) 10 wt.% Pd-coated SFG75.

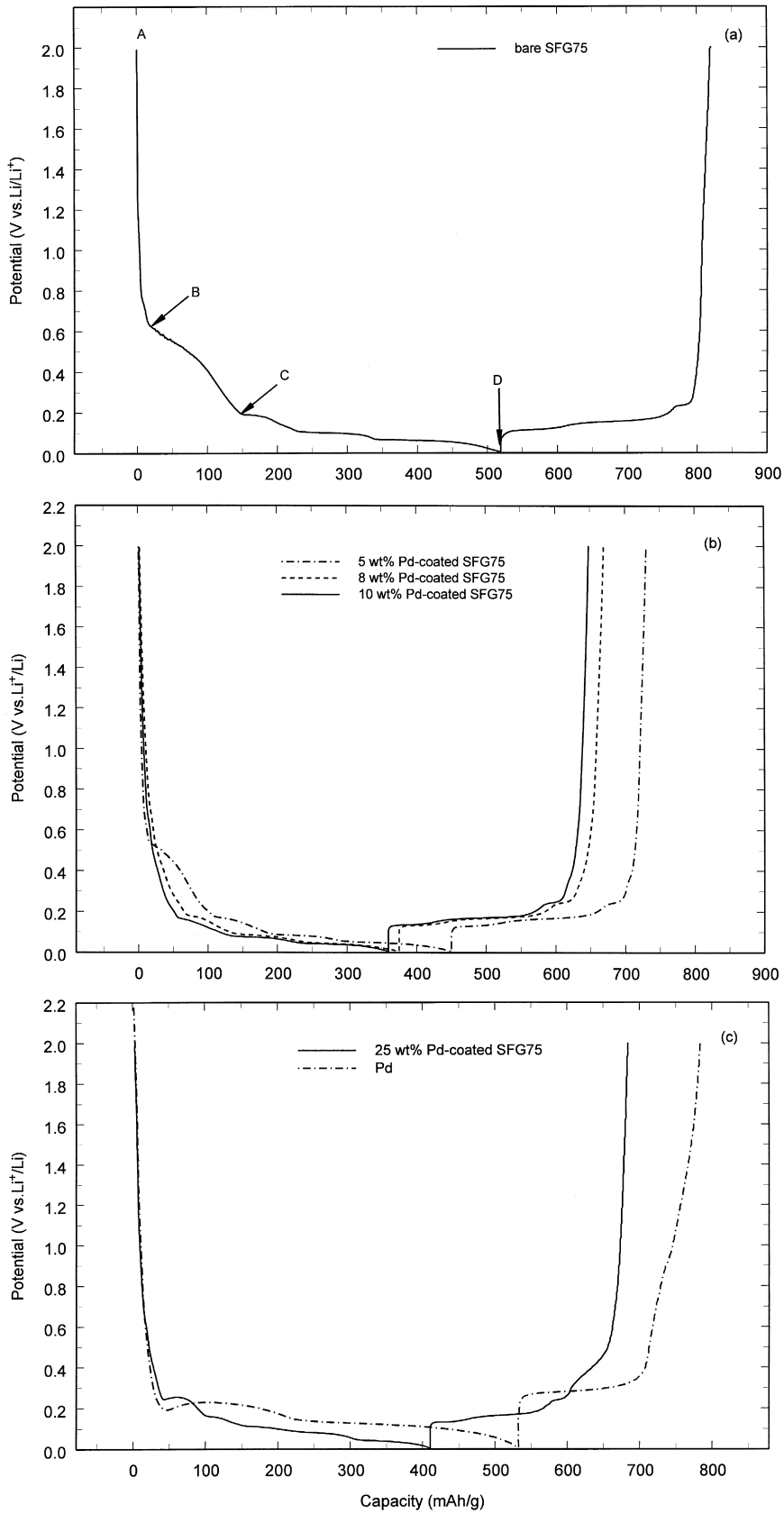

Fig. 2. Initial charge–discharge profiles for (a) bare SFG75, (b) 5, 8 and 10 wt.% Pd-coated SFG75, and (c) 25 wt.% Pd-coated SFG75 and pure palladium.

separator. The electrolyte consisted of 1 M $LiPF_6$ in a 1:1:3 mixture of PC–EC–DMC (EM) and was used as received. After the T-cell was assembled, it remained in the glove box for 30 min to allow the electrolyte to disperse into the porous structure of the graphite anode.

The charge–discharge behavior of the T-cell was investigated using an Arbin Battery Test (BT-2043) system at a current of 0.5 mA (C/8 rate) with cut-off potentials of 0.005 and 2 V vs. Li/Li^+. Cyclic voltammograms were obtained using a scan rate of 0.05 mV/s. The EIS data were collected over the frequency range of 100 kHz to 0.005 mHz with a low ac voltage amplitude of 5 mV, to ensure that the electrode system was under minimum perturbation. In order to stabilize the system, the T-cell was charged and discharged for three cycles between 0.005 and 1.0 V vs. Li/Li^+ using a constant current density of 0.1 mA/cm^2 before the EIS experiments were performed.

Surface images of bare and Pd-coated SFG75 were obtained with a Hitachi S-2500 Delta SEM. The structures of the Pd-coated SFG75 graphites, before and after charging to specified states, were also investigated using a Rigaku 405S5 XRD with CuK_α as the radiation source. The electrical resistances of bare and 10 wt.% Pd-coated SFG75 were estimated using a digital multimeter, with the material (about 0.65 g) pressed into a pellet 0.8 cm in diameter and 6 mm thick by applying either 4.0 or 14.0 $tons/cm^2$ of pressure.

3. Results and discussion

Fig. 1a,b and c display the SEM images of bare SFG75, and 5 and 10 wt.% Pd-coated SFG75, respectively. The bright spots in Fig. 1b were identified as palladium using energy dispersive analysis with X-rays (EDAX). These images show clearly that palladium particles are dispersed over the surface of SFG75, and that the sizes of the palladium particles are on the order of nanometers. Moreover, the particle size does not change upon increasing the amount of palladium from 5 to 10 wt.%, but clearly almost all of the graphite surface is covered by the 10-wt.% palladium coating. The presence of palladium nanoparticles on the surface of graphite also increased the electrical conductivity of the graphite. For example, under a pressure of 4.0 $tons/cm^2$, the electrical resistance for the 10-wt.% Pd-coated SFG75 at 1.1 Ω is smaller than that for the bare SFG75 at 2.1Ω; and upon increasing the pressure to 14.0 $tons/cm^2$, the electrical resistances of both samples decreases, but that for the 10-wt.% Pd-coated SFG75 at 0.6 Ω still remains lower than that for the bare SFG75 at 0.9 Ω. The observed increased conductivity in the presence of 10 wt.% dispersed Pd nanoparticles on the surface of SFG75 is attributed to the larger conductivity of the palladium metal (9.4×10^4 S/cm^2) compared to that of graphite (7.2×10^4 S/cm^2) [19]. This increased conductivity should also reduce the ohmic losses while cycling.

The galvanostatic charge–discharge performance in the first cycle for bare and 5, 8, 10 and 25 wt.% Pd-coated SFG75 is shown in Fig. 2. The curves between the pairs of points, AB, BC and CD, in Fig. 2a exhibit different slopes, which indicates that different reactions/processes are taking place within these potential ranges. According to Winter's classification [5], the region AB above 0.62 V vs. Li/Li^+ corresponds to electrolyte decomposition/solid electrolyte interface (SEI) film formation, the region BC between 0.62 and 0.19 V vs. Li/Li^+ is mainly related to solvated lithium intercalation and reduction, and the region CD below 0.19 V vs. Li/Li^+ is associated with the formation of a lithium–graphite intercalation compound

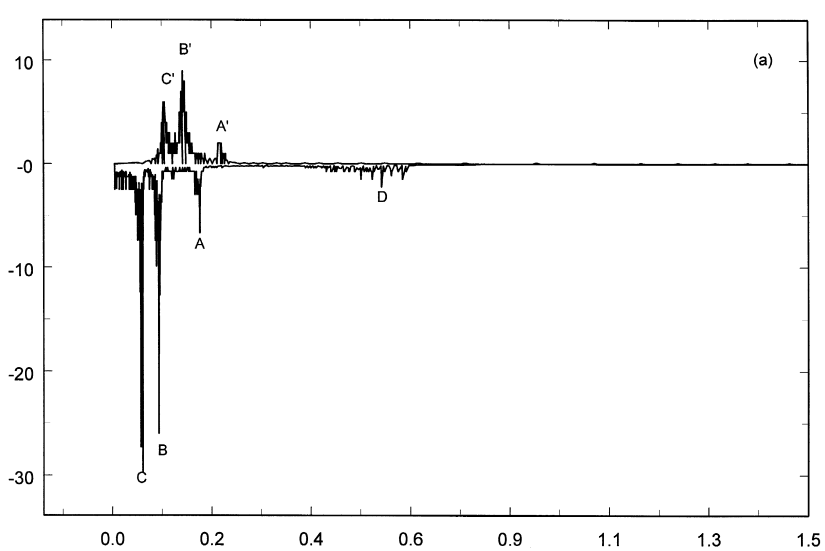

Fig. 3. Derivative capacities as a function of the electrode potential for (a) bare SFG75, (b) 5 wt.%, (c) 10 wt.% and (d) 25 wt.% Pd-coated SFG75, and (e) pure palladium. The data were extracted from Fig. 2. Peaks A, B, C, D, E and F are reduction peaks, and peaks A′, B′, C′ and F′ are oxidation peaks.

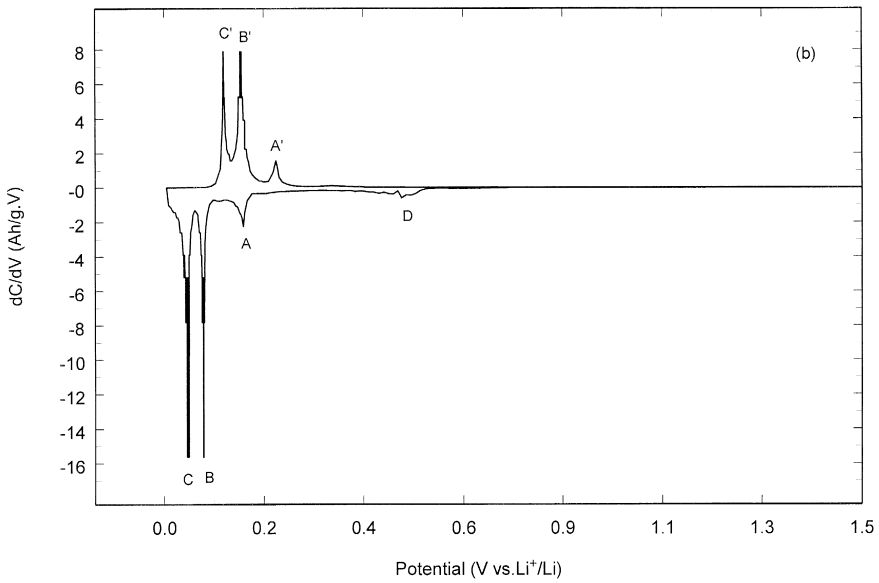

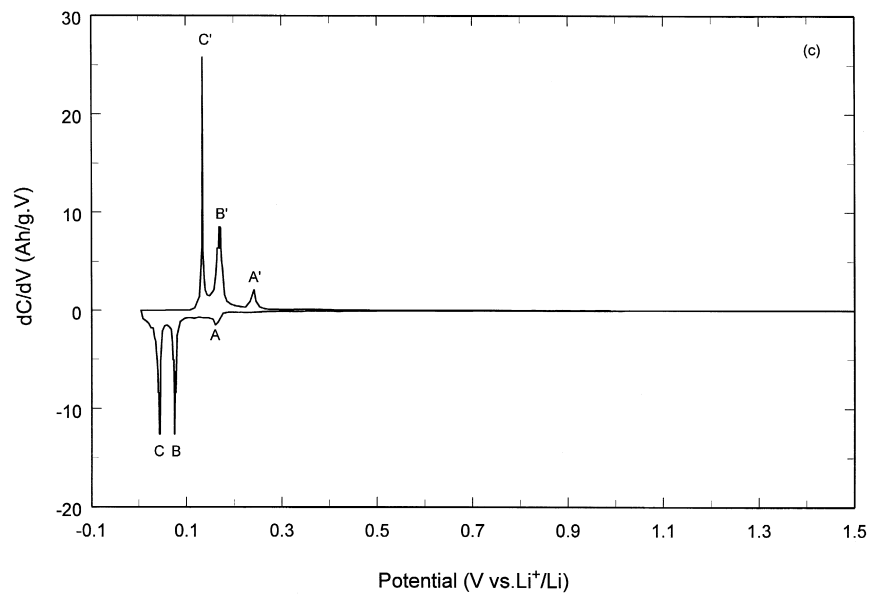

Fig. 3 (*continued*).

(Li-GIC). The capacities arising from electrolyte decomposition and solvated lithium intercalation are irreversible and cannot be recovered during subsequent cycles. This means that for bare SFG75, about 22 mA h/g of capacity is lost above 0.62 V vs. Li/Li^+, and about 133 mA h/g of capacity is lost in between 0.19 and 0.62 V vs. Li/Li^+. This corresponds to 4.2% and 25.6% of the total charge capacity of 519 mA h/g, respectively. Note also that the irreversible capacity related to solvated lithium intercalation and reduction (25.6% of total capacity) is much larger than that associated with SEI film formation (4.2% of total capacity) and dominates the total irreversible capacity. Clearly, bare SFG75 is incapable of preventing solvated lithium intercalation, wherein the reduced lithium compound becomes trapped between the graphene layers of the graphite.

Fig. 2b presents the discharge curve after deposition of 5 wt.% Pd on SFG75. The plateau between 0.19 and 0.62 V vs. Li/Li^+ is still seen but dramatically reduced. The capacity loss in this case is 89 mA h/g, which is 33% lower than that for bare SFG75. However, by further increasing the Pd content on the surface, the plateau is completely eliminated. For example, no plateaus are observed between 0.19 and 0.62 V vs. Li/Li^+ for the 8, 10 and 25 wt.% Pd-coated SFG75 in Fig. 2b and c. These results indicate that solvent cointercalation with the lithium ions is suppressed when a sufficient amount of palladium coats the SFG75 graphite surface. However, when the

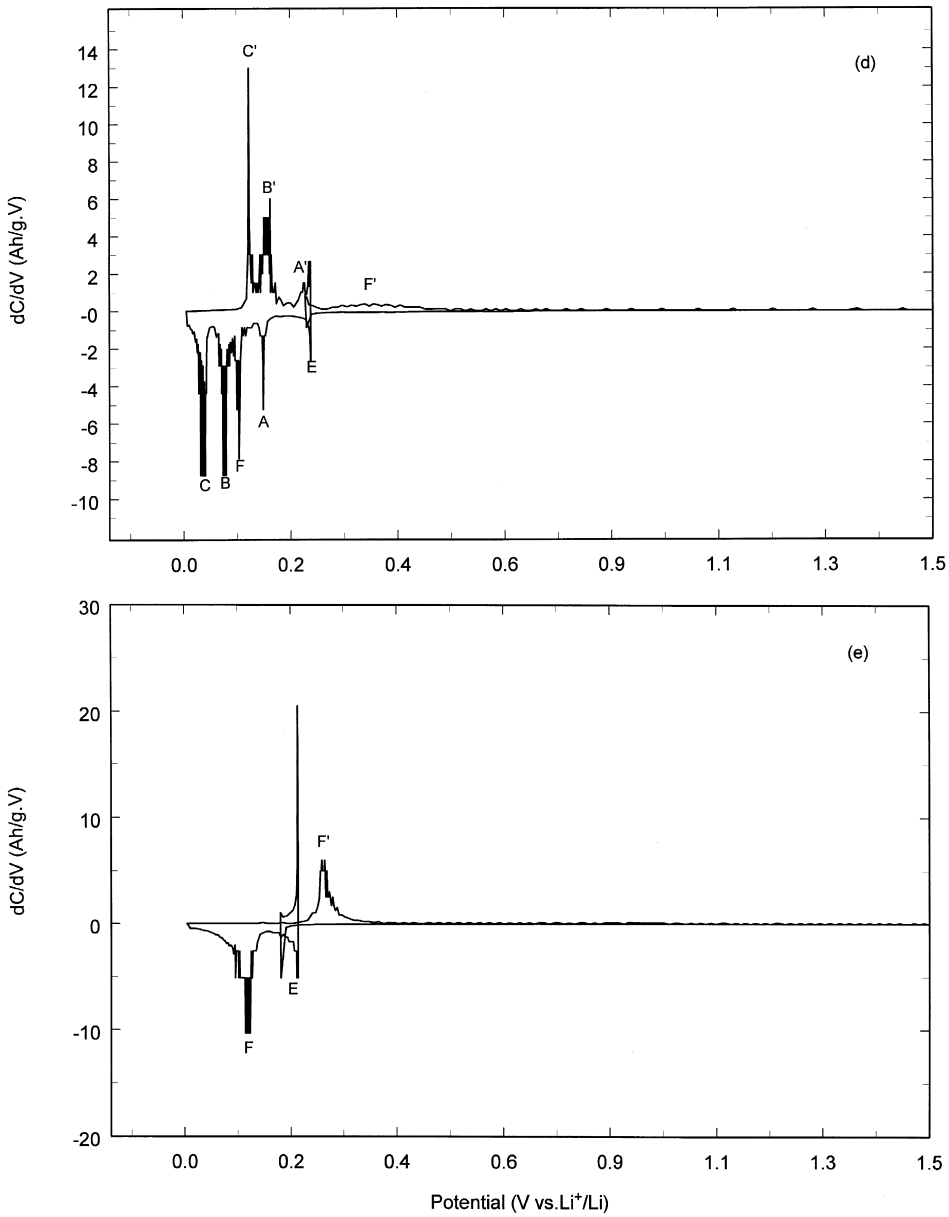

Fig. 3 (*continued*).

amount of palladium deposited on SFG75 increases to 25 wt.%, a new plateau is observed on the charge curve at 0.22 V vs. Li/Li^+. An initial charge–discharge curve of pure palladium powder (0.357 μm, Aldrich) obtained at $C/8$ rate identified this plateau as being unique to palladium metal; this curve is shown in Fig. 2c.

To better understand the difference in the initial intercalation behavior of bare and Pd-coated SFG75, the capacities in Fig. 2 were differentiated with respect to the potential; the resulting curves of dC/dV vs. potential for bare, 5, 10 and 25 wt.% Pd-coated SFG75, and pure palladium are plotted in Fig. 3. Three cathodic peaks (A, B and C), and three anodic peaks (A′, B′ and C′), which characterize the different stages of Li-GIC formation, are revealed in all of these curves. Peak D appears in Figs. 3a and b between 0.4 and 0.62 V vs. Li/Li^+ for both bare and 5 wt.% Pd-coated SFG75, indicating that 5 wt.% palladium is not sufficient to cover the graphite substrate. Hence, solvent intercalation and reduction still occurs on the surface. Fig. 3c shows that a 10-wt.% palladium deposit on SFG75 causes peak D to totally disappear between 0.22 and 0.62 V vs. Li/Li^+. Essentially, the same behavior is observed for the 25-wt.% Pd-coated SFG75 and pure palladium shown in Fig. 3d and e. These results again indicate that when a sufficient amount of palladium coats the graphite surface, the irreversible capacity related to solvated lithium intercalation and reduction is significantly suppressed. The fact that the solvated lithium intercalation takes place mainly on the edge surfaces of graphite rather than on the basal planes of graphite [9] suggests that the marked effect of a palladium coating on suppressing solvated lithium intercalation is due to the palladium parti-

cles depositing on these edge surfaces. A palladium film on the edge surface of graphite may serve as a barrier film that depresses the diffusion of the solvated lithium ions. For bare graphite without a Pd coating, the solvated lithium ions diffuse freely through the entire graphite surface exposed to the electrolyte. However, when palladium is deposited on the graphite, the lithium diffusion path is restricted to the interstitial space between the palladium particles or inside the palladium particles. Since the palladium particles are nanometers in size, the interstitial space between the particles can be presumed to be in the nanometer range also. With this feature, the smaller lithium ions compared to the larger solvated lithium ions can diffuse more easily through the narrowed interstitial space between the palladium particles or inside the particle. Thus, the solvated lithium intercalation into graphite is inhibited when a sufficient palladium coating covers the graphite surface.

Apart from the expected peaks, two additional cathodic peaks (E and F) and one additional anodic peak (F′) manifest in the derivative curves shown in Figs. 3d and e for the 25-wt.% palladium-coated graphite and pure palladium, respectively. Note that the derivative peaks, F and F′, appear in both the charge and discharge curves, while peak E occurs only in the first charge process and does not appear in the discharge process or in subsequent cycles. Clearly, the reduction reaction corresponding to peak E is irreversible, while the reduction/oxidation reactions corresponding to peaks F and F′ are quasi-reversible. To determine the nature of peaks E and F, XRD experiments were conducted on pure palladium.

The XRD patterns for palladium metal are illustrated in Fig. 4 before cycling (curve *a*), and after charging to 0.19 V (curve *b*) and 0.005 V (curve *c*) vs. Li/Li^+. Three sharp peaks are observed in curve *a*, which characterize the crystalline structure of the palladium metal. When the palladium metal is charged to 0.19 V vs. Li/Li^+, the intensities of these three peaks are reduced substantially and new peaks corresponding to Li_2PdO_2 are detected, as shown in curve *b*. Since, peak E appears in Fig. 3d and e at a similar potential, the irreversible reaction in the first cycle can be attributed to the formation of Li_2PdO_2. On continuing to charge this material to 0.005 V vs. Li/Li^+ (curve *c*), the same XRD pattern is obtained but with an increase in the peak intensity corresponding to Li_2PdO_2 formation. No other peaks corresponding to lithium–palladium alloys such as $Li_{1.12}Pd_{2.88}$, $Li_{1.372}Pd_{2.628}$ and $Li_{2.48}Pd_{5.52}$ are detected for these charged states. However, the repetitiveness of peaks F and F′ during every charge–discharge cycle implies that some other lithium–palladium products are being formed. This phenomenon is similar to that which occurs during lithium insertion/extraction in tin metal [18–21], where various Li–Sn compounds are formed, as evidenced by the appearance of redox peaks. However, these alloys are difficult to detect by XRD, similarly to the Li–Pd alloys (compounds) being formed here. Possible reasons are that an amorphous structure or too small of a crystallite size cannot be detected by XRD. Since the potential (0.12 V vs. Li/Li^+) for the formation of Li–Pd alloys is within the range for the formation of Li-GIC, it is important to determine the effect of palladium on the lithium intercalation/deintercalation rate.

To investigate this aspect, CV was carried out on bare and 25 wt.% Pd-coated SFG75, and pure palladium. Fig. 5a shows the CV curves obtained with a scan rate of 0.05 mV/s for bare SFG75 and palladium during the initial cycle. Fig. 5b and c present the CV curves for 25 wt.%

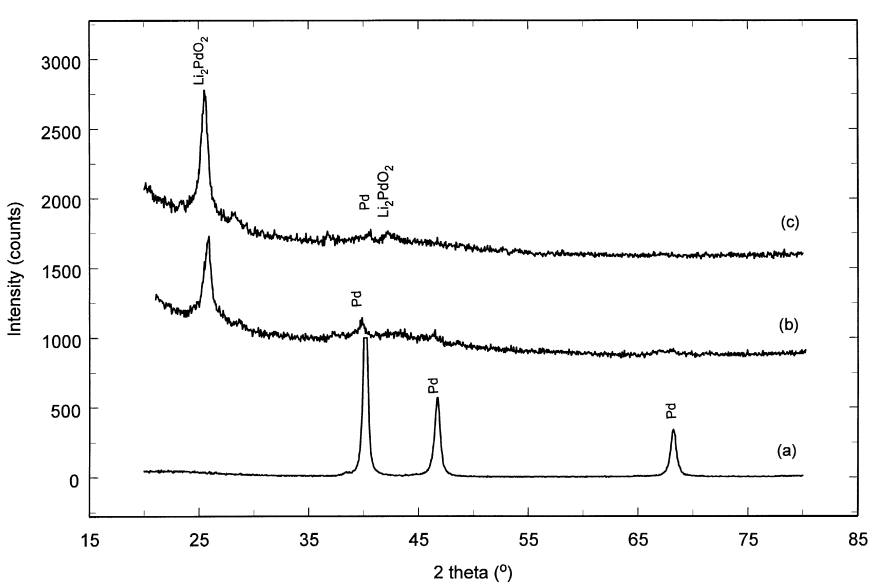

Fig. 4. XRD patterns for (a) palladium metal before cycling, (b) palladium electrode charged to 0.19 V vs. Li/Li^+, (c) palladium electrode charged to 0.005 V vs. Li/Li^+. The electrodes were first galvanostatically charged to the specified potential at C/8 rate and then potentiostatically charged until the current density dropped to 1 μA.

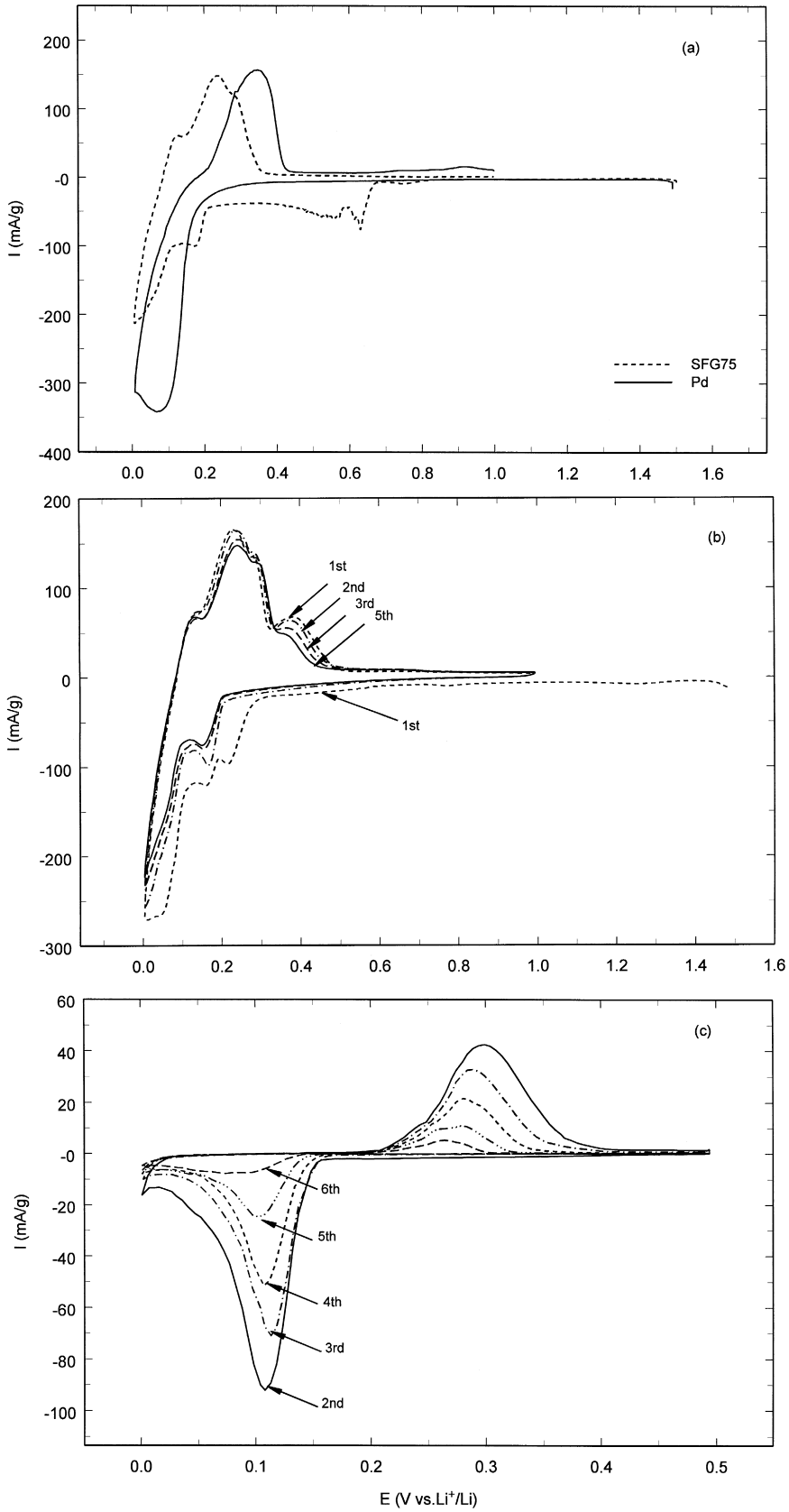

Fig. 5. Cyclic voltammograms for (a) bare SFG75 and pure palladium in the initial cycle with a scan rate of 0.05 mV/s, (b) 25 wt.% Pd-coated SFG75 at various cycles with a scan rate of 0.05 mV/s, and (c) pure palladium at various cycles with a scan rate of 0.01 mV/s.

Pd-coated SFG75 and pure palladium at various cycles and with scan rates of 0.05 and 0.01 mV/s, respectively. The cathodic peak currents corresponding to lithium intercalation into bare SFG75, 25 wt.% Pd-coated SFG75, and Pd are 202, 270 and 334 mA/g, respectively. The anodic peak currents corresponding to lithium deintercalation from bare SFG75, 25 wt.% Pd-coated SFG75, and Pd are 140, 155, 145 mA/g, respectively. These results show clearly that the presence of a palladium coating on graphite increases the amount of lithium inserted into the graphite, and thus increases the charge–discharge capacity. This enhancement agrees with the contribution to the charge capacity observed in Fig. 3d (peak F/F′ corresponding to the formation of a Li–Pd alloy). However, the lithium insertion/extraction peak currents attained with the 25-wt.% Pd-coated SFG75 decreases successively with increasing charge–discharge cycles, as shown in Fig. 5b. For example, the intercalation peak current decreases from 270 mA/g in the first cycle to 223 mA/g in the 4th cycle. Fig. 5c shows that this rapid decrease in the lithium intercalation/deintercalation peak current also occurs with palladium metal, which indicates the formation of a stable Li–Pd alloy that is not capable of cycling reversibly. A similar problem exists for Li–Sn alloys, where severe capacity loses have been reported with cycling for both tin coatings [22] and SnO_2-glass type materials [18–21]. It is thought that density changes and the resulting repeated expansion and shrinkage caused by the insertion and release of lithium [22] leads to the capacity decay with cycling. It appears that Li–Pd alloys suffer from a similar problem, with larger amounts of the palladium coating resulting in more capacity loss and thus less charge–discharge efficiency.

Fig. 6 presents the initial charge capacity and initial charge–discharge coulombic efficiency as functions of the palladium content on the surface of the graphite electrode; this data was extracted from that shown in Fig. 2. The initial charge capacity linearly decreases from 519 to 359 mA h/g and the initial charge–discharge coulombic efficiency substantially increases from 59% to 80.3% as the wt.% Pd increases from 0 to 10 wt.% on SFG75. However, the opposite trend is seen upon increasing the amount of palladium to 25 wt.%. These results are understood in terms of the following three effects from the palladium coating: (i) reduction in the solvated lithium intercalation leading to a decrease in the irreversible charge capacity, (ii) a increase in the irreversible capacity by Li_2PdO_2 formation, and (iii) a continuous decay in the current peaks due to quasi-reversible Li–Pd alloy formation. With less than 10 wt.% palladium coating on the graphite surface, the dominant factor is the prevention of solvated lithium intercalation by the palladium coating. Hence, the total charge capacity, including the irreversible capacity, reduces and the initial charge–discharge efficiency increases because of the palladium content. However, with a 25-wt.% palladium coating on the graphite surface, the dominant factor is the formation of Li–Pd alloys. Therefore, the initial charge capacity, including the irreversible capacity, increases and the charge–discharge efficiency decreases when further increasing the palladium content. The optimum coating obtained in this work is a 10-wt.% Pd coating on SFG75, which provides 359 mA h/g of initial charge capacity and 80.3% of initial charge–discharge efficiency. The cycle life studies shown in Fig. 7 for the various Pd-coated graphite electrodes indicate that the charge–discharge efficiency remains essentially constant with cycling for palladium coatings up to about 10 wt.% (Fig. 7a) and that a further increase in the amount of palladium leads to a decrease in the charge–discharge efficiency (Fig. 7b). Again, a 10-wt.% Pd-coating appears

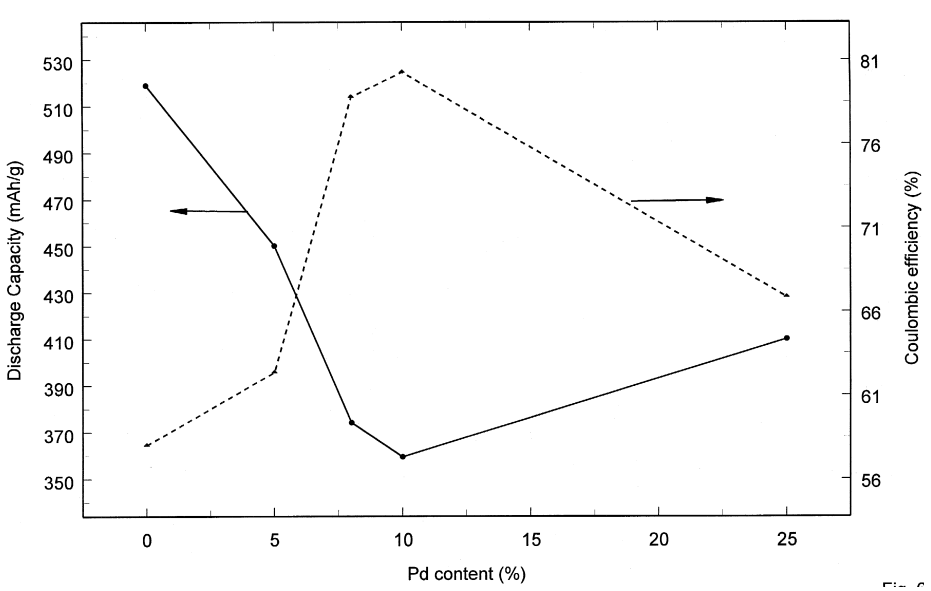

Fig. 6. Initial charge capacities and initial coulomb efficiencies as functions of the palladium content on SFG75. The data were extracted from Fig. 2.

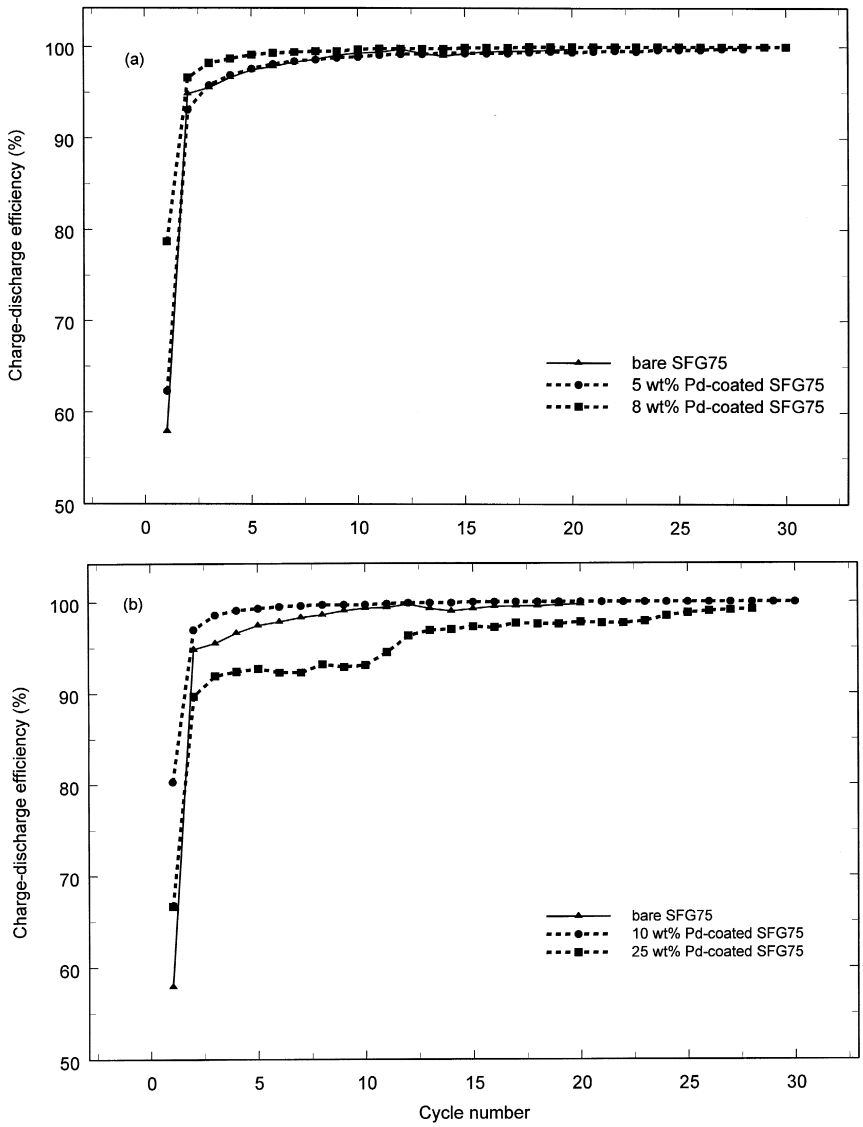

Fig. 7. Charge–discharge efficiencies as a function of the cycle number for (a) bare, and 5 and 8 wt.% Pd-coated SFG75, and (b) bare, and 10 and 25 wt.% Pd-coated SFG75.

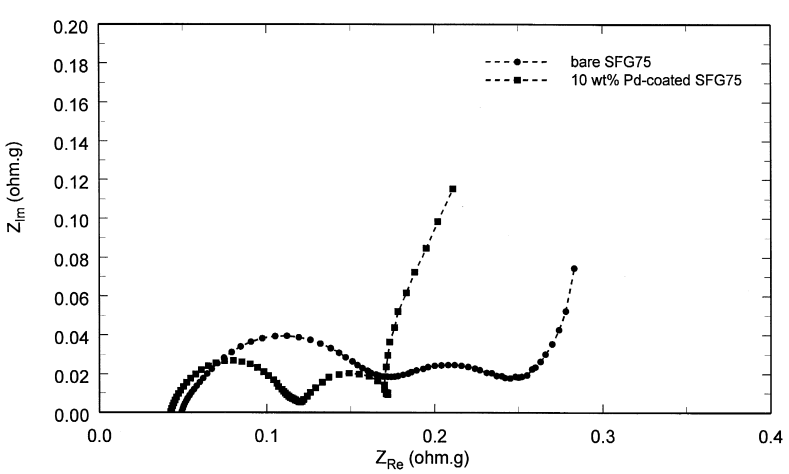

Fig. 8. Nyquist plots for bare and 10 wt.% Pd-coated SFG75.

to be optimum. Cycle life studies for different Pd coatings indicate that the presence of palladium on SFG75 does not hinder the reversible Li intercalation process. According to the EIS results shown in Fig. 8 in terms of Nyquist plots for bare and 10 wt.% Pd-coated SFG75 charged to 0.25 V vs. Li/Li^+, palladium coating on graphite also improves the Li insertion rates. This result is discussed below.

Two semi-circles are observed for both the bare and 10 wt.% Pd-coated SFG75. However, the impedances for the 10-wt.% Pd-coated SFG75 are lower than those for the bare SFG75. The semicircle in the high-frequency region corresponds to the film formation on the surface of graphite, whereas the semicircle in the low-frequency region relates to the Li/Li^+ charge transfer reaction [23]. From these results, it is determined that the surface film resistances on bare SFG75 ($0.15\ \Omega \cdot g$) is twice that on 10 wt.% Pd-coated SFG75 ($0.07\ \Omega \cdot g$). This result is understood in terms of the reduced solvated lithium intercalation and hence the lower amount of nonconductive reduction products formed on the 10-wt.% Pd-coated SFG75 surface. The charge transfer resistance of bare SFG75 ($0.17\ \Omega \cdot g$) is also twice that of the 10-wt.% Pd-coated SFG75 ($0.06\ \Omega \cdot g$). This decreased charge transfer resistance indicates that the presence of palladium coating on graphite is beneficial to the reversible intercalation of lithium, and it may manifest from the increased electrical conductivity of Pd-coated graphite compared to bare graphite.

4. Conclusions

Pd-microencapsulated graphite electrodes containing different palladium contents have been synthesized through the electroless deposition of nanoparticles of palladium on the graphite surface. The presence of the palladium coating dramatically reduces the initial irreversible capacity of the graphite in PC-based electrolyte by suppressing the solvated lithium ion intercalation. This also greatly improves the initial charge–discharge coulombic efficiency. For example, with a 10-wt.% Pd coating on graphite, the initial charge–discharge coulombic efficiency increases from 59% to 80.3%. However, an excess amount of palladium on the graphite surface, such as 25 wt.%, leads to an additional irreversible capacity due to the consumption of lithium by the formation of Li_2PdO_2. EIS results indicate that the palladium coating on graphite not only reduces the surface film resistance but also reduces the charge transfer resistance. The decreased charge transfer resistance is an indication that a palladium coating on graphite facilitates the reversible insertion of lithium into graphite. Overall, the electroless deposition of palladium on graphite is proving to be a very promising approach for reducing the irreversible capacity and improving the charge–discharge performance of graphite used as the negative electrode in Li-ion batteries with PC-based electrolytes.

Acknowledgements

Financial support provided by the DOE Division of Chemical Sciences, Office of Basic Energy Sciences, G. M. De-FG02-96ER 146598, is gratefully acknowledged.

References

[1] J.R. Dahn, A.K. Sleigh, H. Shi, B.M. Way, W.J. Weydanz, J.N. Reimers, Q. Zhong, U. von Sacken, Lithium Batteries, New Materials and New Perspectives, Elsevier, New York, 1993, Pistoia Editor.
[2] R. Fong, U. von Sacken, J.R. Dahn, J. Electrochem. Soc. 137 (1990) 2009.
[3] F. Kong, J. Kim, X. Song, M. Inaba, K. Kinoshita, F. McLarnon, Electrochem. Solid-State Lett. 1 (1998) 31.
[4] Z. Ogumi, M. Inaba, Y. Kawatate, A. Funabiki, T. Abe, Abstract 73, The Electrochemical Society Meeting Abstracts, San Diego, May 3–8, 1998.
[5] M. Winter, P. Novak, A. Monnier, J. Electrochem. Soc. 145 (1998) 428.
[6] P. Arora, R.E. White, M. Doyle, J. Electrochem. Soc. 145 (1998) 3647.
[7] W. Xing, J.R. Dahn, J. Electrochem. Soc. 144 (1997) 1195.
[8] T. Osaka, T. Momma, Y. Matsumoto, Y. Uchida, J. Electrochem. Soc. 144 (1997) 1709.
[9] G. Chung, S. Jun, K. Lee, M. Kim, J. Electrochem. Soc. 146 (1999) 1664.
[10] A.N. Dey, B.P. Sullivan, J. Electrochem. Soc. 117 (1970) 222.
[11] M. Arakawa, J. Yamaki, J. Electroanal. Chem. 219 (1987) 273.
[12] E. Peled, C. Menachem, D. Bar-Tow, A. Melman, J. Electrochem. Soc. 143 (1996) L4.
[13] R. Takagi, T. Okubo, K. Sekine, T. Takamura, Denki Kagaku 65 (1997) 333.
[14] T. Takamura, K. Sumiya, Y. Nihijima, J. Suzuki, K. Sikine, Mater. Res. Soc. Symp. Proc., Pittsburgh 496 (1997) 557.
[15] T. Takamura, Y. Nishijima, K. Sekine, Presented at the Electrochemical Society Meeting, Spring 97, Montreal, Abstract No. 74 (1997) 86.
[16] K. Nishimura, H. Honbo, S. Takeuchi, T. Horiba, M. Oda, M. Koseki, Y. Muranaka, Y. Kozono, H. Miyadera, J. Power Sources 68 (1997) 436.
[17] H. Honbo, S. Takeuchi, H. Momose, K. Nishimura, T. Horiba, Y. Muranaka, Y. Kozono, Denki Kagaku 66 (1998) 939.
[18] K. Nishimura et al., Presented at the Electrochemical Society Meeting, Spring 97, Montreal, Abstract No. 76 (1997) 88.
[19] R.C. West, Handbook of Chemistry and Physics, 52nd edn., The Chemical Rubber, Cleveland, OH, 1971.
[20] W. Liu, X. Huang, Z. Wang, H. Li, L. Chen, J. Electrochem. Soc. 145 (1998) 59.
[21] Y. Idota, T. Kubota, A. Matsufuji, Y. Maekawa, T. Miyasaka, Science 276 (1997) 1395.
[22] I.A. Courtney, J.R. Dahn, J. Electrochem. Soc. 144 (1997) 2045.
[23] A. Funabiki, M. Inaba, Z. Ogumi, J. Electrochem. Soc. 145 (1998) 172.
[24] P. Yu, J.A. Ritter, R.E. White, B.N. Popov, J. Electrochem. Soc., 147 (2000) 1280.